J Neurophysiol 109: 1202–1213, 2013.
First published November 28, 2012; doi:10.1152/jn.00830.2012.

Spectral inputs and ocellar contributions to a pitch-sensitive descending neuron in the honeybee

Y.-S. Hung,[1,2,3] J. P. van Kleef,[3,4] G. Stange,[3] and M. R. Ibbotson[1,2,3]

[1]*National Vision Research Institute, Australian College of Optometry, Carlton, Victoria, Australia;* [2]*Department of Optometry and Vision Science, University of Melbourne, Parkville, Victoria, Australia;* [3]*Australian Research Council Centre of Excellence in Vision Science, Research School of Biology and Eccles Institute of Neuroscience, John Curtain School of Medical Research, Australian National University, Canberra, Australian Capital Territory, Australia; and* [4]*Department of Electrical Engineering and Computer Science, College of Engineering, University of California Berkeley, Berkeley, California*

Submitted 17 September 2012; accepted in final form 26 November 2012

Hung YS, van Kleef JP, Stange G, Ibbotson MR. Spectral inputs and ocellar contributions to a pitch-sensitive descending neuron in the honeybee. *J Neurophysiol* 109: 1202–1213, 2013. First published November 28, 2012; doi:10.1152/jn.00830.2012.—By measuring insect compensatory optomotor reflexes to visual motion, researchers have examined the computational mechanisms of the motion processing system. However, establishing the spectral sensitivity of the neural pathways that underlie this motion behavior has been difficult, and the contribution of the simple eyes (ocelli) has been rarely examined. In this study we investigate the spectral response properties and ocellar inputs of an anatomically identified descending neuron ($DNII_2$) in the honeybee optomotor pathway. Using a panoramic stimulus, we show that it responds selectively to optic flow associated with pitch rotations. The neuron is also stimulated with a custom-built light-emitting diode array that presented moving bars that were either all-green (spectrum 500–600 nm, peak 530 nm) or all-short wavelength (spectrum 350–430 nm, peak 380 nm). Although the optomotor response is thought to be dominated by green-sensitive inputs, we show that $DNII_2$ is equally responsive to, and direction selective to, both green- and short-wavelength stimuli. The color of the background image also influences the spontaneous spiking behavior of the cell: a green background produces significantly higher spontaneous spiking rates. Stimulating the ocelli produces strong modulatory effects on $DNII_2$, significantly increasing the amplitude of its responses in the preferred motion direction and decreasing the response latency by adding a directional, short-latency response component. Our results suggest that the spectral sensitivity of the optomotor response in honeybees may be more complicated than previously thought and that ocelli play a significant role in shaping the timing of motion signals.

direction selective; spectral tuning; *Apis mellifera*; ocelli; optomotor responses

MOST ANIMALS, INCLUDING HUMANS, reflexively track the movement of the whole visual field with their eyes, heads, and/or bodies during self-movement. Reflexive tracking responses can occur within six degrees of freedom, three translational (forward/backward, up/down, side-to-side) and three rotational (roll, pitch, or yaw). These behaviors are referred to as optomotor responses in insects (e.g., Schlieper 1927). The most commonly encountered equivalents in vertebrates are reflexive ocular following, or optokinetic, eye movements (e.g., Ibbotson et al. 2007). Optomotor and optokinetic responses attempt to reduce image motion on the retina caused by unintentional movements of the head and body. During normal flight insects hold a steady course for short periods interspersed with rapid saccade-like head and body movements that are intended to change course direction (Boeddeker and Hemmi 2010; Boeddeker et al. 2010; van Hateren and Schilstra 1999). This mode of flight has an important role in separating the optic flow that occurs across the retina into rotational and translational components (Karmeier et al. 2006; Kern et al. 2005; Lindeman et al. 2008). During translational flight bees attempt to keep their retinal image stable using optomotor head and body turning reflexes. During flight, external influences such as air currents can move the animal away from its intended course or gaze direction. During the translational phases any unintentional head and body movements will induce image rotation, which requires counteractive body rotations in the direction of image motion, thus compensating for the unintentional deviation. For this reason, it has been established that optomotor neurons have highly selective tuning to detect specific rotations of the body around various rotational axes (e.g., roll, yaw, and pitch: Ibbotson and Goodman 1990; Krapp and Hengstenberg 1996; Wertz et al. 2008).

In bees the optomotor response has been used to study the mechanisms of motion and color vision (Künze 1961; Schlieper 1927). The latter study found that the honeybee optomotor response appeared to be color blind and was highly sensitive to color contrast (also see Kaiser and Liske 1974). Kaiser and Liske (1974) measured the spectral sensitivity of the honeybee optomotor response for horizontal motion presented in the ventral eye region and found that it matched the spectral sensitivity of the green photoreceptors (peak around 540 nm). Thus it has been suggested that honeybees use only one photoreceptor type (green) to drive the motion detectors that provide input to the optomotor system, thereby explaining the apparent color blindness of the optomotor response (Kaiser 1975). Experiments measuring the horizontal optomotor responses of flies similarly suggest exclusive input from one spectral class of photoreceptors (R1–R6; Yamaguchi et al. 2008), but this was very recently challenged by experiments demonstrating the involvement of other spectral classes of photoreceptors (R7 and R8; Wardill et al. 2012).

Extracellular recordings from motion-sensitive interneurons in the honeybee and fly optic lobes show that although their spectral sensitivity tuning is very similar to the green photoreceptor, there is in some cases a secondary peak at wavelengths of 340–380 nm (Autrum and von Zwehl 1964; Kaiser

Address for reprint requests and other correspondence: M. R. Ibbotson, National Vision Research Institute, Australian College of Optometry, Corner Keppel and Cardigan Sts., Carlton, Victoria 3053, Australia (e-mail: mibbotson@nvri.org.au).

1975; McCann and Arnett 1972; Srinivasan and Guy 1990). These physiological data suggest that some motion-sensitive interneurons in the brain have inputs from short-wavelength photoreceptors. However, it is not clear that all direction-selective neurons in the optic lobes provide input to optomotor responses (Hertel and Maronde 1987), so the link between physiology and behavior is weak.

Descending neurons that connect the central brain with thoracic motor neurons and respond in a direction-selective fashion to visual motion have been reported in a range of insects, including flies (Wertz et al. 2008), butterflies (Singarajah 1988), locusts (Kien 1974; Rowell and Reichert 1986), mantids (Yamawaki and Toh 2009), dragonflies (Olberg 1981a, 1981b, 1986), and honeybees (Hung et al. 2011; Ibbotson 1991a, 1991b). It is believed that these descending neurons are on the optomotor pathway, because their visual sensitivity to motion matches that of optomotor responses (Ibbotson and Goodman 1990; Wertz et al. 2008). In honeybees, the descending neurons were also reported to be direction selective and to have specialized optic flow-detecting capabilities (Goodman et al. 1987, 1990, 1991; Ibbotson 1991a, 1991b; Ibbotson and Goodman 1990). In the present study, we conducted intracellular recordings from a prominent motion-sensitive descending neuron in the honeybee to investigate the possibility that short-wavelength photoreceptors contribute to the neural circuitry underlying optomotor motion responses. We describe the visual responses of the cell for both short and green wavelengths of light. The relative contributions from the ocelli and compound eyes to the directionality of the cell were also tested.

MATERIALS AND METHODS

Experimental Preparation

Experiments were conducted on honeybees, *Apis mellifera*, that had been actively foraging. Hives were situated at the Australian National University in Canberra, Australia. Each bee was lightly anesthetized by cooling at 4°C for about 20 min. After its legs were removed, the bee was placed horizontally (dorsal side up) on a metal holder, and the head and thorax were secured with a 3:1 mixture of beeswax and violin resin. A chlorinated silver wire was then inserted into the thorax to serve as the indifferent electrode for intracellular electrophysiological recordings (see below). The ventral nerve cord was exposed from the dorsal side of the neck, between the suboesophageal and prothoracic ganglia, so that a recording electrode could be vertically inserted into it. Once prepared, the bee was left for 15 min before any recordings were made for the temperature to recover to room levels (22–24°C).

Honeybee motion-sensitive descending neurons have been described and classified previously according to their neuronal morphology (Goodman et al. 1987; Ibbotson 1991a, 1991b). The classification scheme and terminology described in those works are used throughout this study. The recordings and results presented in this article are focused on one identifiable motion-sensitive descending neuron, named $DNII_2$. Through random selection during recordings, this particular neuron was recorded from most frequently and subsequently filled with dye, thus providing a strong statistical basis for comparisons between preparations (from 110 anatomically identified neurons in 110 preparations, $DNII_2$ was filled on 22 occasions).

Microelectrodes were pulled using a P-97 Flaming/Brown puller (Sutter Instruments) from borosilicate glass capillaries (GC100TF-10, Harvard Apparatus). The electrode tips were filled with 10% Lucifer yellow CH (lithium salt; Invitrogen) in 1% LiCl solution and then backfilled with 1 M LiCl solution, producing impedances of ~100 MΩ in honeybee saline (111.22 mM NaCl, 3.35 mM KCl, 1.37 mM $CaCl_2$, and 1.89 mM Na_2CO_3).

The microelectrode was inserted vertically into the exposed ventral nerve cord and lowered gently using a mechanical micromanipulator. Once the electrode was in position, the microelectrode holder was tapped lightly to penetrate the cell membrane. When a stable resting potential was detected, flashed wide-field visual stimuli were used to stimulate the eyes to confirm that the recorded cell was a visual neuron.

Visual Stimulation

Neurons were tested for visual responses quantitatively by using custom visual stimuli produced on two devices.

Monitor displays. VSG Series 2/5 stimulus generators (Cambridge Research Systems, Cambridge, UK) were used to control stimuli on three monochromatic CRT display monitors. Stimuli were presented on gamma-corrected green-emitting monitors running at 198 Hz (57 cd/m^2 mean luminance, 600 × 400 pixels; Clinton Monoray) at a viewing distance of 20 cm. The monitors used a DP104 phosphor with peak spectral emission at 565 nm (emitting from 520 to 610 nm). The viewable regions of the screens measured 35 × 32 cm and were positioned such that one covered the frontal visual field and the other two were oriented at 90° to each other to cover the left and right visual fields, respectively. Stimuli were either high contrast (0.8) sine-wave gratings that could be moved back and forth at any angle on the screen or rotating windmill patterns (4 black and 4 white sectors, all of the same width). A range of spatial and temporal frequencies could be used. For the data presented on flow field sensitivity, we standardized presentations such that the standard gratings moved at 4 Hz and windmill rotation was 1 rotation per second, thus providing 4 full black-white cycles per second. The spatial frequency of the grating patterns was 0.2 cycles per degree.

LED display. A two-dimensional wide-field LED array, described in Berry et al. (2006), was used to present visual stimuli during electrophysiological experiments. Figure 1*A* shows a schematic diagram of the LED display. Briefly, the display consisted of 9 columns of LEDs, and each column consisted of 12 pairs of short-wavelength (peak emission at 380 nm; Roithner Lasertechnik) and green LEDs (peak emission at 530 nm; Roithner Lasertechnik). The emission spectra of the LEDs are shown, along with the photoreceptor spectral sensitivities of the three photoreceptor types in the compound eye and the two receptor types in the ocellar retinas (Fig. 1, *B* and *C*). The emission spectrum of the green LEDs covered the peak region of the spectral sensitivity of honeybee green photoreceptors in the compound eyes (Fig. 1*B*) and the upper spectral region of the blue-green-wavelength receptors in the honeybee ocellus (Fig. 1*C*). It should also be noted that the lower wavelength cutoff for the green stimulator was such that it coincided with the upper cutoff of the compound eye blue photoreceptor and did not overlap at all with the ocellar UV receptor (Fig. 1, *B* and *C*). Therefore, the green LEDs provided stimuli that were almost exclusively stimulating the green (or blue-green in the ocelli) photoreceptors. The situation for the short-wavelength stimulus was far more complicated. The problem is that there is no practical short-wavelength emission spectrum that would not provide simultaneous stimulation to the UV, blue, and green photoreceptors in the compound eyes or to the UV and blue-green photoreceptors in the ocelli. This is because all the green and blue receptors generate relatively strong responses at all practical low wavelengths (Fig. 1). We selected a wavelength of light that peaked at 380 nm to provide stimulation for the UV and blue photoreceptors of the compound eyes. The theoretical quantum catch of the chosen LED is shown in Fig. 1, *D* and *E* (for calculation, see below).

The quantum catch for photoreceptors represents the number of quanta that are absorbed by a certain photoreceptor type and is widely used as input for calculations and models of color vision (e.g., Kelber

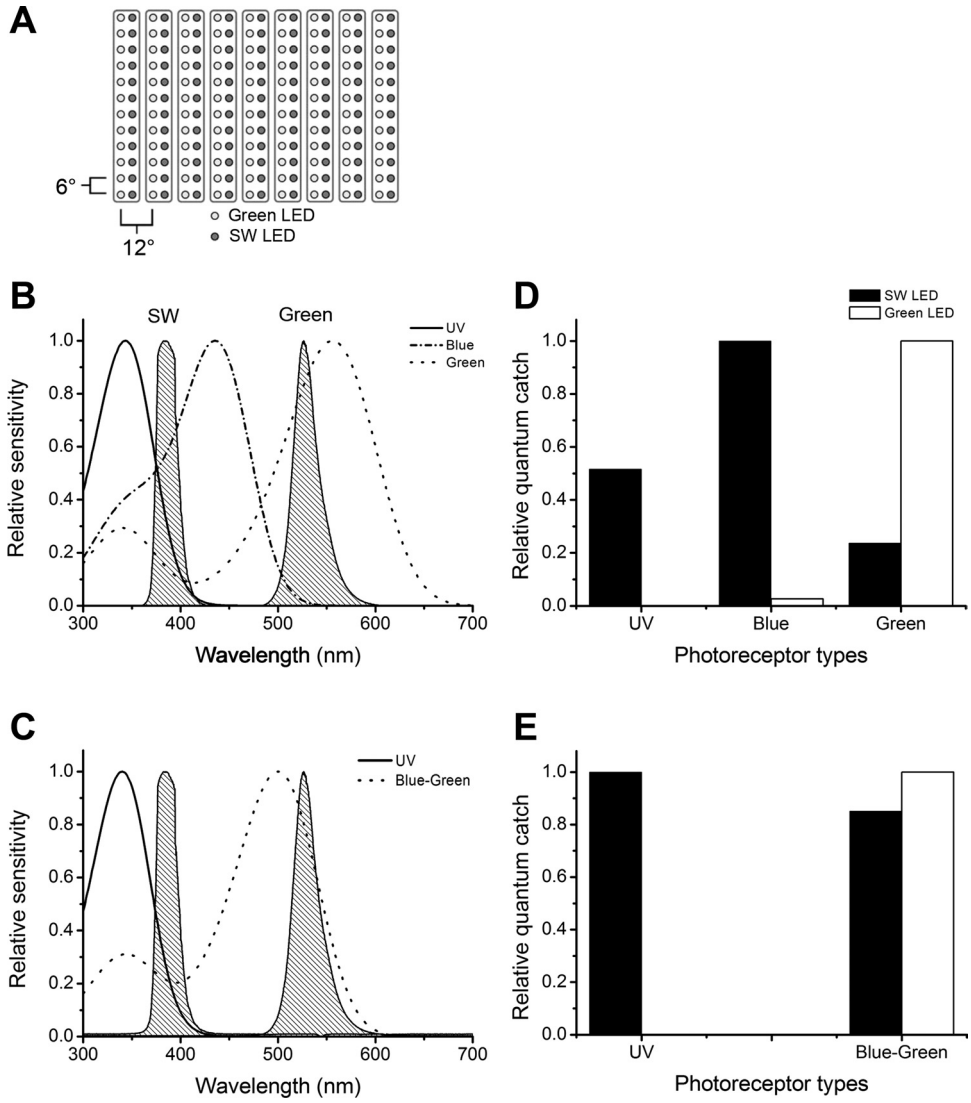

Fig. 1. *A*: schematic diagram of the wide-field LED display [from Fig. 1 of Berry et al. (2006) with kind permission from Springer Science+Business Media, copyright Springer-Verlag 2006]. The distance between LEDs is 6° in the vertical direction and 12° in horizontal direction. *B*: spectral sensitivities for the 3 photoreceptor types (UV, blue, green) in the honeybee compound eyes are shown. Shaded areas show the emission spectra of the 2 LEDs used in our spectral stimulus: green and short wavelength (SW). *C*: spectral sensitivities of the 2 photoreceptor types in the ocelli are shown, with the emission spectra of the LEDs superimposed in gray. *D* and *E*: relative quantum catch for the photoreceptors in the compound eyes and ocelli, respectively.

1999; Kelber et al. 2003). In this study, the relative quantum catch (Q) for a photoreceptor type i (where in honeybee, i = UV, blue, blue-green, or green receptors) to the stimulation used in the experiments was calculated from the integral of the spectrum weighted by the receptor sensitivity curves:

$$Qi = \int_{300}^{700} S(\lambda)P(\lambda)d\lambda, \qquad (1)$$

where $S(\lambda)$ is the emission spectrum of the LED and $P(\lambda)$ is the spectral sensitivity curve of the photoreceptor. The spectral sensitivity curves of the honeybee (P) were generated using a vitamin A_1 template described by Stavenga et al. (1993) and by considering the photoreceptor peak sensitivity (alpha band) at the appropriate wavelength for each receptor type (Autrum and Zwehl 1964; Menzel and Blakers 1976; Menzel et al. 1986). It is worth noting that Menzel and Blakers (1976) found variability in peak UV sensitivity of up to 30 nm in bee retina. It is therefore possible that the quantum catch calculations could be slightly different from bee to bee.

The estimated quantum catches for the three receptors in the compound eyes for both the short-wavelength and green stimuli are presented in Fig. 1*D*. The green stimulus almost exclusively stimulates the green receptor. The short-wavelength stimulus provides the largest quantum catch for the blue receptor and 50% of that value for the UV receptor. The relative quantum catch for the green receptor was 20% of that for the blue receptor. The estimated quantum catches for the two receptor types in the ocelli are presented in Fig. 1*E*. The green stimulus activates only the blue-green receptor. The short-wavelength stimulus provides approximately equal quantum catches for the UV and blue-green receptors in the ocellar retina.

LEDs were arranged at 6° intervals on the circumference of a circle; both the short-wavelength and green sources were arranged at intervals of 6° in elevation and 12° in azimuth. Therefore, the display provided a range of −33° to 33° in elevation and −48° to 48° in azimuth wide-field visual stimuli. The honeybee head is positioned at the center of this circle. The intensity of each LED was controlled by individual voltage-to-current driver amplifiers and calibrated using either short-wavelength or green-sensitive photodiodes (EPD-365-0/2.5, Electro Optical Components, and series 15-5T, Centronic, respectively). The LEDs are driven by individual voltage-to-current-converting driver amplifiers, and each driver amplifier is independently controlled via a 32-channel digital-to-analog (D/A) converter with 14-bit resolution (AD5532HS, Analog Devices). The converter features a digital sample-and-hold on each channel so that pixels are only refreshed if they have changed value. The converter is driven via a microcontroller (Isopod, NewMicros), which communicates with the personal computer (PC) via a parallel port. Data from the PC are converted by the microcontroller into the serial format required by the D/A converter. The display was refreshed at a rate of 625 Hz. The PC

was run on the Linux operating system (Debian), with a real-time module (RTAI) for synchronous data acquisition and control, interfaced with MATLAB for higher level functions. After calibration, the intensity of the short-wavelength LEDs had a maximum flux of $\approx 1.2 \times 10^{14}$ photons·cm^{-2}·s^{-1} at $\lambda = 380$ nm, and the green LEDs had a maximum flux of $\approx 0.9 \times 10^{14}$ photons·cm^{-2}·s^{-1} at $\lambda = 530$ nm, at the position of the honeybee head.

Visual stimulus protocols. With the use of the LED display described above, two different types of visual stimuli were employed in this study: wide-field flashed stimuli and directional motion stimuli. To examine the ocellar contribution to the descending neuron responses, recordings were made with visual stimuli presented to both the compound eyes and the ocelli simultaneously and to the compound eyes alone (i.e., with the ocelli covered). The ocelli were covered by a handmade small cap. The cap was made of a small ($\sim 3 \times 3$ mm) piece of aluminum foil on one side together with an equal-sized piece of black paper on the other side. The foil was bent on the sides so that it covered the ocelli completely. The small cap was placed over the ocelli with the aluminum foil side out. The aluminum foil side acted to block any coming light while the black surface facing the ocelli absorbed any light that may have scattered from under the outer rim of the cap. It proved impossible to reliably and reversibly cover the compound eyes while leaving the ocelli uncovered. Stray light always managed to stimulate some part of the compound eye whatever the covering technique used. In contrast, it was possible, due to their small size, to reversibly cover the ocelli using the small cap while leaving the compound eyes unaffected.

Flashed stimuli. The arrays of short-wavelength and green LEDs were modulated independently with a constant short-wavelength and green background set at 50% of their respective maximum intensities. Modulation of short-wavelength and green intensity above and below this background was controlled by two independent sequences, one driving all short-wavelength LEDs simultaneously and one driving all green LEDs simultaneously. Increments (80% maximum intensity) or decrements (20% maximum intensity) of either the short-wavelength or green channel above or below the mean background were 38 ms in duration and separated by 1 s. The sequence of the flashes was always as follows: short-wavelength increment, green increment, short-wavelength decrement, and then green decrement (see Fig. 7*A*).

Directional stimuli. Directional stimuli consisted of either single bars or gratings moving either vertically or horizontally at different speeds. Vertically moving bars were 6° wide, and horizontally moving bars were 12° wide. The bars could take several forms. We did not mix LED stimulation; i.e., when a green background was used, the bars also used green LEDs. Similarly, when a short-wavelength background was used, the bars used short-wavelength LEDs. When a particular wavelength was in use (green or short), the LEDs for the other wavelength were inactive. Bright bars consisted of a moving bar of LEDs that had higher brightness than the background (positive contrast bars). Dark bars consisted of a moving bar of LEDs that had lower brightness than the background (negative contrast bars). The contrast of the bars was either +0.82 (positive contrast) or −0.82 (negative contrast). Bars were presented at 12 increasing speeds, from 100 to 3,750°/s, and then at decreasing speeds so that two samples of the response for each speed were obtained. This sequence could then be repeated to obtain additional experimental repeats for each speed. Bar stimuli at the speed of 341°/s with 10 different contrasts (from +0.82 to −0.82) were also applied in some experiments. Previous studies on $DNII_2$ showed that its motion response decayed (adapted) over several seconds but was relatively constant over the first 500 ms (Ibbotson and Goodman 1990). Thus, to avoid the possibility of motion adaptation influencing the results, each of the visual stimuli was presented for less than 500 ms in this study.

Data Analysis

The electrode potential was amplified (model 5A, Getting Instruments), displayed on an oscilloscope, and recorded digitally at a sampling rate of 5 kHz on a PC using a 14-bit analog-to-digital converter (PCI-DAS1001, Measurement Computing). The recorded data were analyzed offline using MATLAB. First, an action potential was judged to have occurred if the difference between consecutive measurements of the membrane potential (dV) exceeded a threshold. This threshold was set at three times the standard deviation of dV over the entire recording. Spikes were determined to occur at the zero crossing of dV that occurs immediately following the point at which dV exceeds the threshold. The spike density functions were calculated by convolving the spike arrival times with a Gaussian filter with a width at 1/e of the maximum of 5 ms.

For the bar stimulus, the response rate was calculated as the number of spikes that occur during the stimulus time minus the spontaneous activity of the cell and normalized by the maximum response in the preferred direction. The spontaneous activity for each trial was estimated from the average spike rate during the 500-ms period before stimulus onset.

All the data presented were tested for normality using the Lilliefors goodness-of-fit test of composite normality before further statistical analysis. The data were found to be normal ($P > 0.05$). This was also confirmed through inspection of quantile-quantile plots of the data.

Anatomy

After the completion of intracellular recording, cells were filled with Lucifer yellow CH (lithium salt; Invitrogen) by iontophoretic injection of 5–10 nA (negative injection) for at least 15 min. Following a general histological protocol outlined by Hung et al. (2011), the honeybee brain was optically sectioned by confocal microscope (LSM Pascal, Zeiss). The stacks of images were processed using offline Zeiss confocal software (Axiovision) to reconstruct and generate the three-dimensional (3-D) models of the neurons.

RESULTS

Recordings were made from 300 descending neurons, and from this population 110 were filled and anatomically identified. Among the identified cells, 22 cells from separate preparations were classified as $DNII_2$. The anatomic characteristics of this neuron are already well established (Ibbotson and Goodman 1990). For easy cross-referencing with earlier studies and to provide a modern 3-D reconstruction of the neuron, the morphology of the neuron, as viewed dorsally and laterally is shown on the basis of optical sectioning of fluorescent dye-filled tissue (Fig. 2). $DNII_2$ lies on the posterior side of the brain with the cell body located on the lateral edge of the protocerebral bridge, close to the calyx of the mushroom bodies (see Fig. 2*B* for honeybee brain anatomy). The trunk of the dendritic arbors with fine branches projects to both halves of the brain in the posteromedial protocerebrum, dorsal to the oesophageal foramen (Fig. 2*A*). The neuron descends into the thoracic ganglia, where it sends branches to both halves of the ganglia, with the branches confining themselves to the most dorsal regions of the ganglia (Fig. 2*C*). With the use of the 3-D model of the honeybee nervous system previously developed in our laboratory (Berry and Ibbotson 2010), the location of the $DNII_2$ neuron is shown to scale in the 3-D reconstruction of the brain and prothoracic ganglion (Fig. 2*D*).

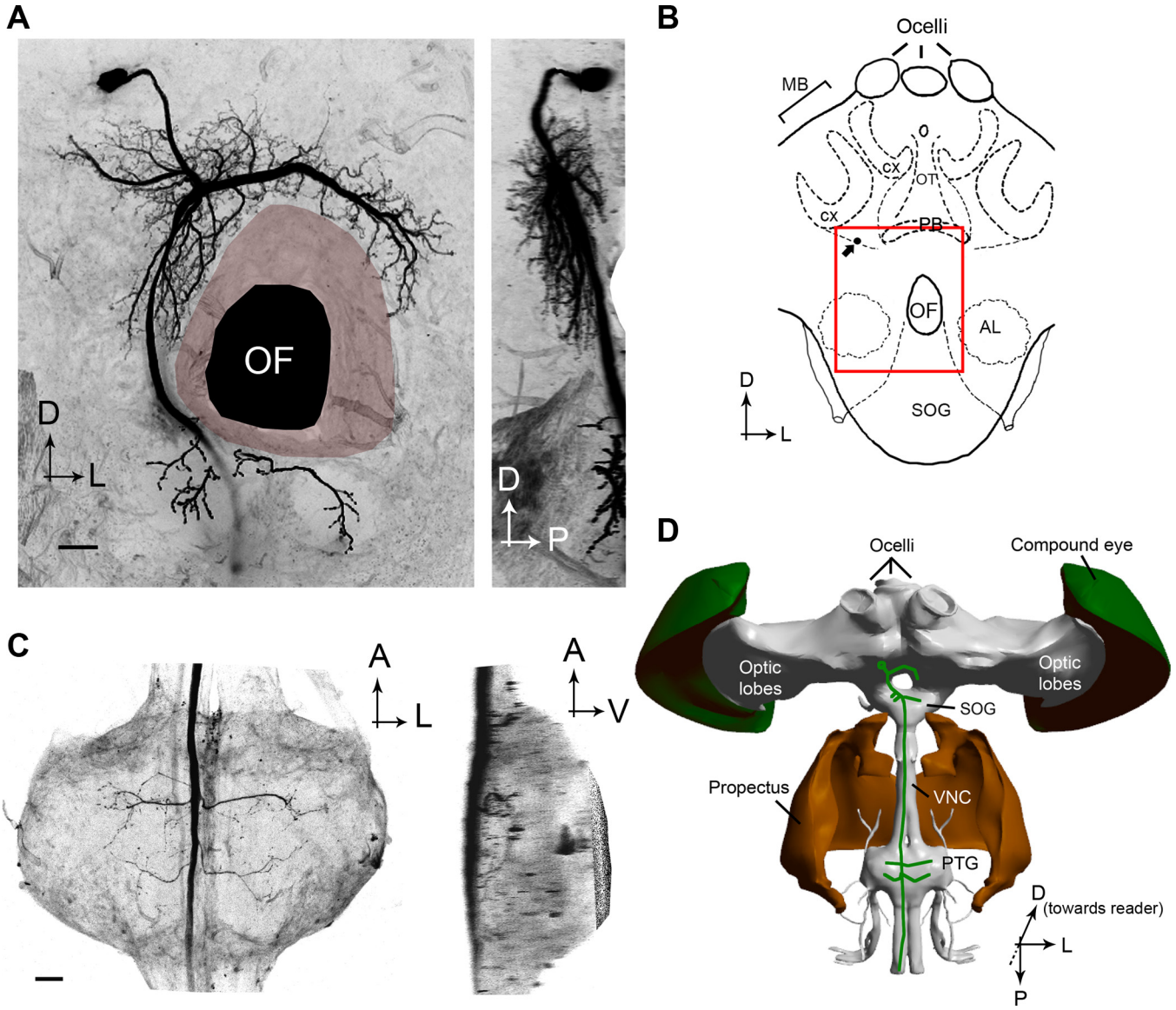

Fig. 2. *A*: anatomy of $DNII_2$, as viewed from the posterior and lateral perspectives. *B*: schematic diagram of a honeybee midbrain region showing the basic brain anatomy of the honeybee. The locations of the mushroom bodies (MB) are indicated, and the calyx (cx) for each MB is shown using dashed lines. The red box shows the area of optical sectioning shown in *A*, and the small black arrow indicates the location of the cell body of $DNII_2$. *C*: dorsal and lateral views of the prothoracic ganglion with a single fill of $DNII_2$, showing its bilateral branches. Note from the lateral view that the axonal branches terminate at shallow locations in the ganglion. *D*: 3-dimensional (3-D) reconstruction of the bee nervous system showing the brain and prothoracic ganglion from the dorsal perspective. The green schematic drawing shows the location and size of $DNII_2$. The 3-D model of the honeybee nervous system was developed in our laboratory (Berry and Ibbotson 2010). AL, antennal lobe; OF, oesophageal foramen; OT, ocellar tracks; PB, protocerebral bridge; SOG, suboesophageal ganglion; VNC, ventral nerve cord; A, anterior; V, ventral; D, dorsal; P, posterior. Scale bars, 100 μm.

Optic Flow Sensitivity

Using three green-emitting, fast-phosphor monitors running at 198 Hz and positioned to cover the frontal and lateral regions of the eyes, we showed that $DNII_2$ was very selective for detecting optic flow fields that simulated the movement patterns that occur during pitch rotations of the head. The following data are from five identified neurons (error bars show the average across the 5 mean responses). Optimal responses were induced when the frontal grating stimulus moved upward and the lateral windmill stimuli rotated clockwise on the animal's right and counterclockwise on the animal's left (Fig. 3). This optic flow pattern simulates a pitch rotation in which the front of the head turns downward. Upward motion frontally and no stimuli laterally also induced large responses, but they were significantly smaller than those to the former stimulus (*t*-test, $P = 0.019$; Fig. 3). Selective upward frontal motion over either the right or left eye generated responses that were not significantly smaller than for frontal binocular stimulation (left eye covered, *t*-test, $P = 0.125$; right eye covered, *t*-test, $P = 0.119$; Fig. 3). When the rotating windmill stimuli were moved in their respective optimal directions without frontal stimulation, the cell produced small responses (5–10 spikes/s) that were significantly higher than the spontaneous activity (*t*-test, $P < 0.01$) but considerably smaller than the response amplitudes during combined lateral and frontal stimulation (Fig. 3). The opposite direction of motion during all conditions that had

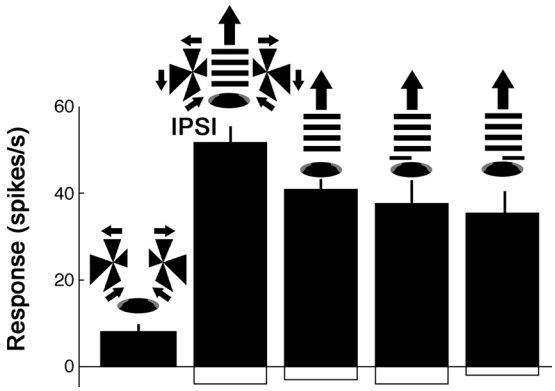

Fig. 3. Histograms showing (from *left* to *right*) the response amplitudes of responses to simulated downward pitch of the animal with lateral-only stimulation, simulated downward pitch with frontal and lateral stimulation, simulated downward pitch with binocular frontal-only stimulation, simulated downward pitch with the left eye covered, and simulated downward pitch with the right eye covered. Schematics at *top* show the stimulus. Filled bars show the number of spikes per second above the mean spontaneous rate for upward image motion (mean and SD from 5 identified $DNII_2$ neurons). Open bars show the number of spikes per second below the mean spontaneous rate for motion in the nonpreferred direction.

frontal stimulation led to inhibition of the spontaneous activities of the cells (open bars in Fig. 3). Lateral-only stimulation with the windmill patterns in the anti-preferred direction did not generate inhibition of the background activity of the cell in any preparation (note lack of open bars in Fig. 3). $DNII_2$ did not respond significantly to horizontal image motion on any screen in any preparation (data not shown; also see Ibbotson and Goodman 1990).

Spectral Sensitivity of Motion Responses

Having established that $DNII_2$ has selective optic flow sensitivities to upward grating movements when a green-only stimulus is used, we began using the LED-based stimulus, which was always frontally positioned so that it could provide optimal motion stimulation to both the compound eyes and ocelli. We present responses for the cell to stimulation in its preferred (upward) and anti-preferred (downward) directions of motion in Fig. 4, *A–C*.

The static green background generated relatively high ongoing spiking activity (Fig. 4*A*). Conversely, a static short-wavelength background was associated with far less ongoing spiking activity (Fig. 4*B*). The difference in mean activity level between these two cases was significant in all recordings (*t*-test, $P < 0.01$). For both the green and short-wavelength backgrounds, movement of a dark bar across the screen (contrast: −0.8) generated large spiking responses for upward motion and reductions of background firing during downward image motion (Fig. 4, *A* and *B*). When we moved bright bars across the screen (contrast: 0.8), direction-selective responses with similar response patterns and temporal profiles were observed. Speed tuning using moving bars was tested in eight recorded neurons. Speeds ranging from 270 to 3,750°/s were tested. Figure 4*C* shows the mean normalized speed tuning functions for the recorded neurons for upward (solid lines) and downward motion (dashed lines). The cells responded over a wide range of speeds for moving green (solid symbols) and short-wavelength bars (open symbols) bars. The recordings provide evidence for two key findings: *1*) stimulation with moving green and short-wavelength bars generates responses with similar amplitudes across the same wide range of speeds for the two colors; and *2*) the peak velocity tuning is in the range from 270 to 600°/s, with a peak at 340°/s. At speeds between 600 and 1,000°/s, short-wavelength stimulation generated significantly larger responses than green stimulation (*t*-test, $P < 0.01$).

Complete contrast-response functions were tested in four identified $DNII_2$ cells for both positive and negative contrasts

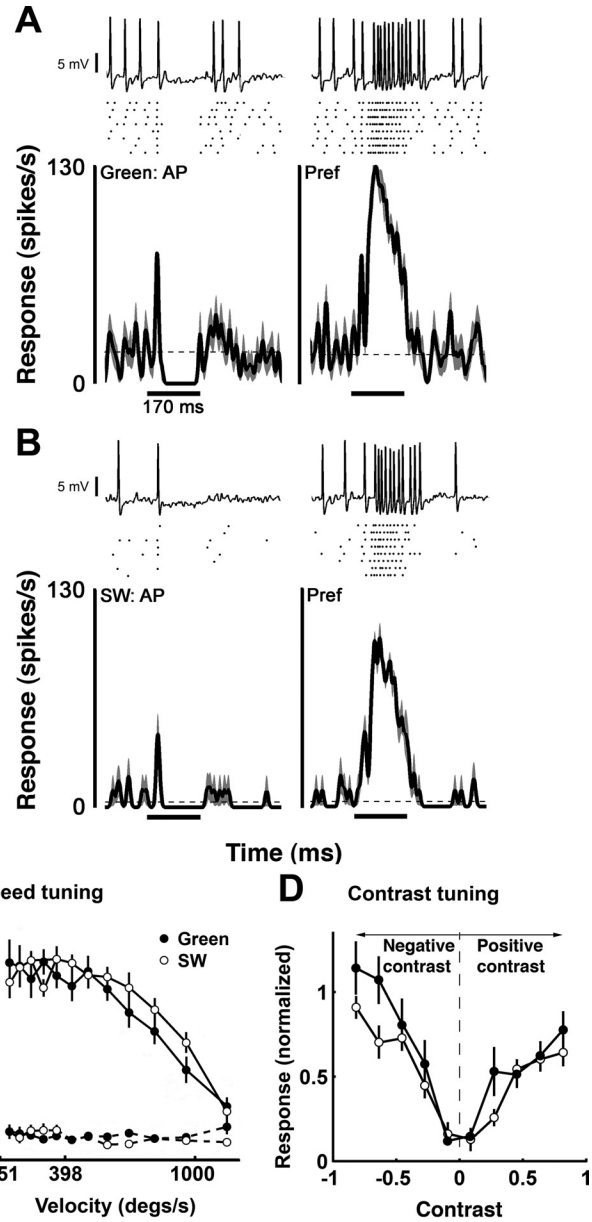

Fig. 4. *A*: spike density functions (*bottom*; with SE in gray) and associated raster plots (*middle*) for a dark bar moving over a green background in the anti-preferred and preferred directions. At *top*, a single raw trace clearly demonstrates the action potential waveforms. AP, anti-preferred direction; Pref, preferred direction. *B*: the same style of plots for a dark bar moving across a SW background. Note that spontaneous activity is larger with the green background, but responses to motion (total response rate minus mean spontaneous rate) are similar for the green and SW stimuli. *C*: speed tuning functions for the preferred (solid lines) and anti-preferred directions (dashed lines) for the green and SW stimuli. *D*: contrast-response functions for negative and positive contrast for the green and SW stimulus. Error bars are SE.

(contrast range: 0.08 to 0.8). The cells were tested with the bar stimulus moving at the optimal angular velocity (340°/s). Figure 4*D* shows the normalized mean responses from the four identified $DNII_2$ neurons. Responses were normalized to the maximum response to the short-wavelength stimulus. An ANOVA test was applied to verify the interactions between different test conditions: contrast, contrast polarity (negative or positive contrasts), and test spectrum (short-wavelength or green). There was no significant interaction between conditions ($F < 2$, $P > 0.1$), so the effects of the test conditions on the normalized response were independent of each other. A significant effect of contrast was found, because for both positive and negative contrasts, the response amplitude increased when contrast increased [$F_{(4,140)} = 28$, $P < 0.0001$]. Responses to negative contrasts for both green and short-wavelength stimulation had larger amplitudes compared with the positive contrast condition. The differences between the response amplitudes for the two contrast polarities were significant [$F_{(1,140)} = 15$, $P < 0.0001$].

Ocellar Contribution

To test the origins of the green and short-wavelength inputs, we conducted identical experiments but with the ocelli covered (i.e., only compound eye stimulation). $DNII_2$ gave clearly different results when the ocelli were occluded. When both the compound eyes and ocelli were stimulated with a moving bar, the response amplitude was ~5% higher than when the compound eyes were stimulated alone across a range of 11 tested speeds. The increase was very small but significant [$F_{(1,160)} = 6.46$, $P = 0.012$]. When the compound eyes were stimulated alone, $DNII_2$ showed a strong response to the short-wavelength (shown) and green bar stimuli during preferred-direction motion that was characterized by a relatively slow, smooth increase in firing rate soon after motion in the preferred direction began (Fig. 5*A*, *right*). Anti-preferred-direction motion generated very few spikes (Fig. 5*A*, *left*). In contrast, when both the compound eyes and the ocelli were stimulated simultaneously with motion in the preferred direction, there was a short-latency transient response that was characterized by highly time-locked spikes, as is very clear from the raster plots (Fig. 5*B*, also see Fig. 4, *A* and *B*). Motion in the anti-preferred direction sometimes generated a spike soon after motion onset, then a period with no spikes, and, finally, a small response soon after motion terminated (Fig. 5*B*, *left*). For all of the stimulus conditions outlined above, stimulation with green bars led to the same effects. The initial short-latency time-locked response was observed during both preferred and anti-preferred directions of motion (Fig. 5*B*, circle with arrow). However, the spikes were very reliable during motion in the preferred direction and much more variable between trials for motion in the anti-preferred direction. Therefore, when we calculated the spikes per second in a short 10-ms time window centered on the transient response, the amplitudes of the responses were significantly larger for the preferred direction of motion (*t*-test, $P < 0.01$, Fig. 5*C*). There were no initial, transient responses observed when the cell was stimulated with horizontal motion for any color (data not shown). Collectively, these results show that the response observed when both the ocelli and compound eyes are stimulated is a combined response that includes an initial ocellar response that has very short latency and is highly transient, and a more prolonged response that originates from the compound eyes. The initial ocellar response is directionally biased, with the response in the preferred direction being more reliable than that in the anti-preferred direction. The compound eye response has lower latency and is highly direction selective, generating robust excitation for upward image motion and a complete suppression of spikes for downward motion.

Given that the ocellar contribution always occurred first, we measured the latencies of the responses. Figure 5*D* shows the results of a careful examination of the time courses of both the compound eye component (Fig. 5, triangles) and the transient ocellar component (Fig. 5, circles) to short-wavelength (open symbols) and green wavelength bar movements (filled symbols) in the preferred direction at three test speeds (938, 469, and 313°/s). The data presented were from eight anatomically identified cells. For all three test speeds the response latency for the ocellar transient is 25–30 ms. Moreover, there is no significant difference between the latencies of the initial ocellar response for short-wavelength and green stimulation (*t*-test, $P > 0.01$). The compound eye component, on the other hand, showed longer latencies for all speeds when the ocelli were uncovered. With both the compound eyes and ocelli stimulated with the green bars, the response latencies were 60–70 ms across the 3 image velocities, whereas when the ocelli were covered, the latencies were between 50 and 75 ms [$F_{(1,95)} = 7.29$, $P = 0$]. This slight increase in time to peak for the compound eye-dominated response probably relates to the time-locked inhibitory phase that immediately follows the time-locked ocellar spikes. This transient inhibitory phase is clearly evident in the spike raster plots and spike density functions shown in Figs. 4 and 5.

Removal of the ocellar input also impacted on the directional properties of $DNII_2$ in a more subtle manner. Downward motion leads to a reduction in the spontaneous activity of $DNII_2$. Immediately after the period of inhibition we typically observed an excitatory burst of action potentials when both the compound eyes and ocelli were stimulated (Fig. 6*A*, also clearly shown in Figs. 4, *A* and *B*, and 5*B*). Interestingly, when the ocelli were covered, this burst of action potentials did not occur (Fig. 6*B*). This change in activity occurred for both green and short-wavelength stimulation and further suggests that the ocelli are integrated in some fashion into the directional circuitry that generates responses in $DNII_2$. To measure the postinhibitory response quantitatively, an 80-ms time window was used in the period immediately following the removal of the stimulus. For a wide range of image speeds, the means and standard errors of the responses during this window are shown for five identified cells (Fig. 6, *C* and *D*). When the ocelli were uncovered, an excitatory rebound response with a peak of around 20 spikes/s was generated after motion in the anti-preferred direction (Fig. 6*C*). When the ocelli were occluded, there was no elevation in activity in the poststimulus time window for motion in the anti-preferred direction (Fig. 6*D*). These responses were the same regardless of whether the bars were short-wavelength or green [$F_{(1,160)} = 0.46$, $P > 0.1$]. There was no postinhibitory response evident for motion in the preferred direction in any of the paradigms, so this situation is not described.

Figure 7 shows a typical response to short-wavelength and green brightness increment flashes. With the use of 38-ms flashed stimuli, $DNII_2$ generated robust and very brief re-

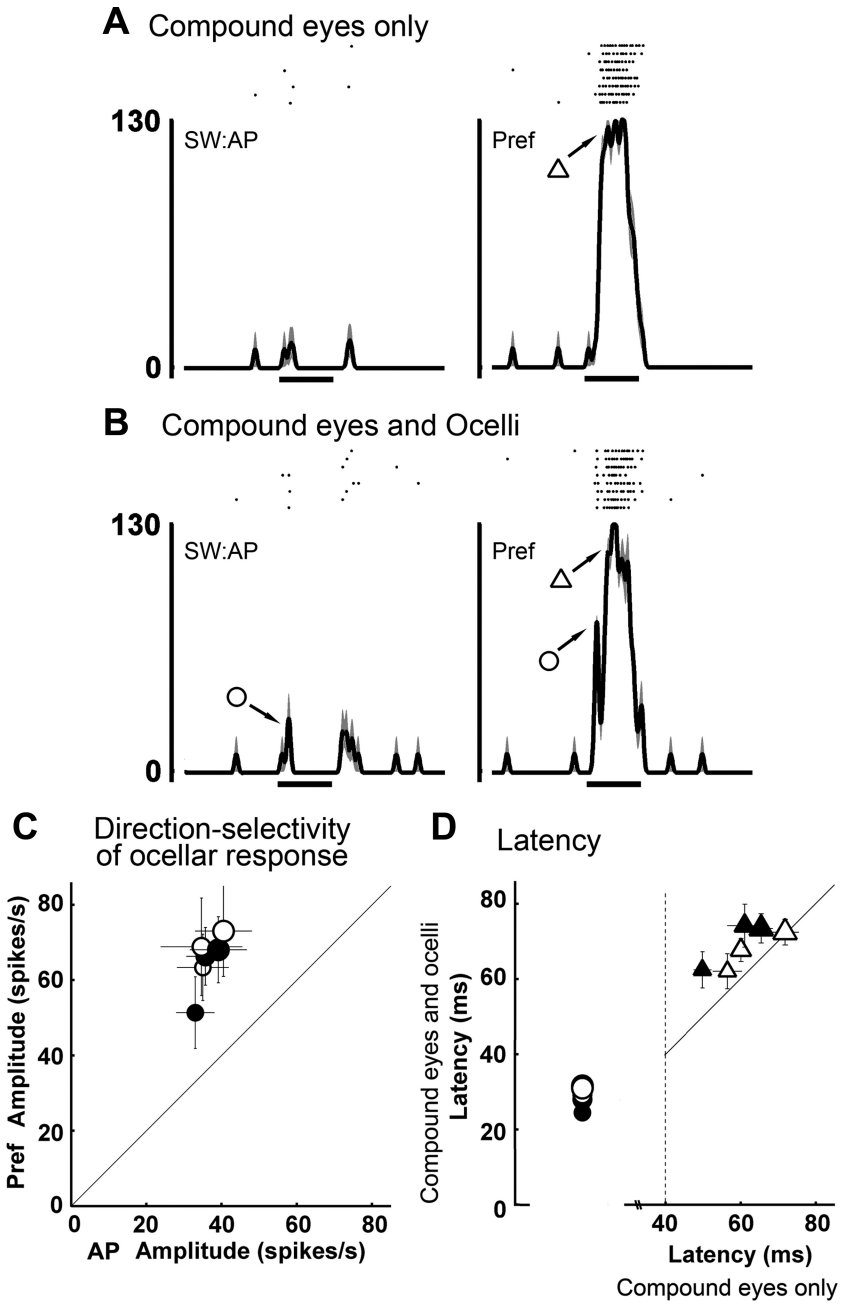

Fig. 5. *A* and *B*: spike density functions and associated raster plots for a dark bar moving over a SW background in the anti-preferred and preferred directions when only compound eyes were stimulated (*A*) and when compound eyes and ocelli were stimulated simultaneously (*B*). The cell has a strong excitatory response (triangles) to preferred-direction motion in both conditions. When both the compound eyes and ocelli were stimulated simultaneously, an initial transient response was observed (circles) for both the anti-preferred and preferred directions. *C*: response amplitudes of the transient responses to preferred-direction motion plotted as functions of the responses to anti-preferred-direction motion. The amplitudes of the preferred-direction responses are significantly larger than those of the anti-preferred-direction responses (*t*-test, $P < 0.01$). SW, open symbols; green, solid symbols. *D*: scatter plot of the response latencies ($n = 8$) to different colored moving bars at 3 different velocities. The triangles show the latencies of the main excitatory response, and the circles show the latencies of the initial transient response during preferred-direction motion. When both the compound eyes and ocelli were stimulated, the latencies were slightly longer than when only the compound eyes were stimulated. However, in both cases the latencies of the excitatory responses were >40 ms (dashed line). The initial transient responses were only observed when the compound eyes and ocelli were stimulated simultaneously. These data are therefore plotted only against the *y*-axis. The latencies of the initial transient responses were shorter (<40 ms) compared with the main excitatory responses.

sponses to brightness increments and decrements (for summary data see Fig. 8). These responses were equally robust during short-wavelength or green stimulation (*t*-test, $P > 0.05$; Fig. 8). When the ocelli were covered, the response amplitudes significantly decreased [$F_{(1,84)} = 13.5$, $P < 0.01$] and, in the case of green brightness increments, there were no responses in 40% of cells tested (Fig. 8, squares). Thus the compound eyes appear to provide input via both short- and green-wavelength receptors, but the ocelli may provide a particularly large contribution to the detection of green brightness increments.

DISCUSSION

In the 1970s Kaiser and colleagues (Kaiser and Liske 1974; Kaiser 1975) established that, for the honeybee, the behaviorally measured spectral sensitivity of the optomotor response almost exactly matched that of the green photoreceptors found in the bee retina (Autrum and Zwehl 1964; Menzel and Blakers 1976; Menzel et al. 1986). This suggested that the optomotor response was exclusively driven by the green photoreceptors. It has long been suggested that motion processing is, and should be, "colour blind" (Srinivasan 1985) and that motion-sensitive interneurons receive inputs from only one class of photoreceptor (e.g., Zhang and Srinivasan 1993; Yamaguchi et al. 2008). Presently, we report the response characteristics of a descending neuron that is tuned to detect the optic flow associated with pitching body movements. It is tuned to detect vertical upward motion in the frontal regions of the eyes and receives excitatory drive from both the green and short-wavelength regions of the spectrum. The neuron responds across a wide range of image speeds, as is common in the optomotor systems of very diverse

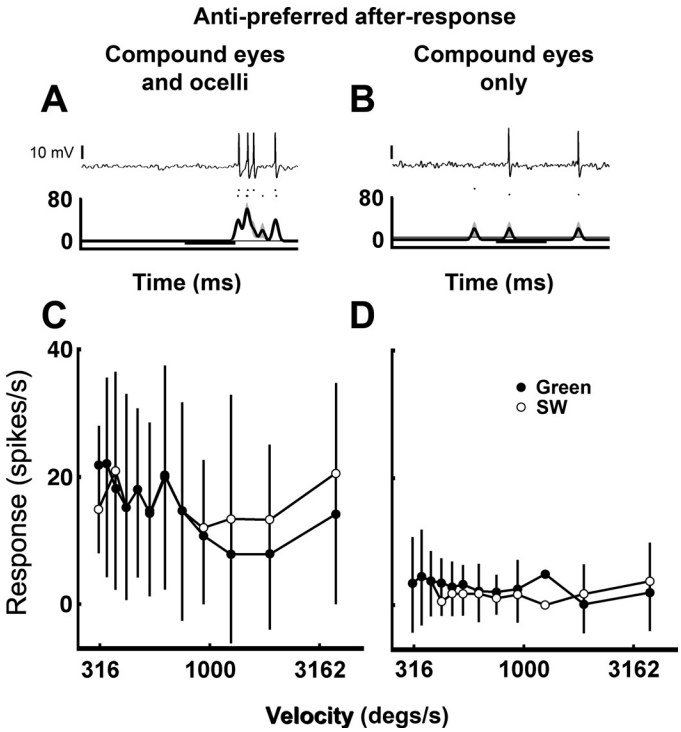

Fig. 6. *A* and *B*: responses to anti-preferred-direction motion using the green LEDs (*top*, a single trace showing action potentials; *middle*, raster plot; *bottom*, spike density function). After anti-preferred-direction motion, there was usually a burst of action potentials when the compound eyes and ocelli were both uncovered (*A*). When the ocelli were covered, the poststimulus response never occurred (*B*). With both types of eyes uncovered, the amplitude of the poststimulus response was not significantly different across a wide range of image speeds (*C*). With only the compound eyes seeing the stimulus, there was no poststimulus response. In this case, the mean firing rate was equal to that of the spontaneous activities of the cells across many speeds (*D*).

species (Ibbotson and Price 2001). Of central importance to the present report, the results suggest that there is a non-green photoreceptor input to the optomotor system of the bee. Although we cannot rule out the possibility that the UV beta peak of the green photoreceptor contributes to the directional response of $DNII_2$, the cell responses to flashed stimuli showed that the short and green-wavelength flashed responses were not significantly different in amplitude (*t*-test, $P > 0.05$). Because the calculations of the theoretical quantum catch (see Fig. 1, *B–D*) suggest that the beta peak of the green photoreceptor could not alone explain the results, the data very strongly suggest that the neuron receives both green and short-wavelength inputs. On the basis of our experiments, we cannot deduce whether this input occurs spatially across the entire retina, but it certainly occurs in the frontal region of the eyes. We can make the prediction that vertical optomotor responses, particularly those driven from the frontal visual field, are both green and short-wavelength sensitive in the bee.

Three spectral classes of photoreceptors have been identified in the compound eyes of honeybees, the so-called green, blue, and UV channels (Fig. 1). They peak at 556, 436, and 344 nm, respectively (Menzel and Blakers 1976; Peitsch et al. 1992). The green LED was capable of selectively stimulating the green channel because the blue photoreceptor channel has virtually no sensitivity above 500 nm. However, virtually any stimulator emitting a wavelength in the UV range will also activate the blue and green channels because they have substantial sensitivity at short wavelengths. Therefore, it is not possible, from the available data, to distinguish whether the input at short wavelength arose from the UV or the blue channel, or both, on the basis of compound eye stimulation. It is very clear that the short-wavelength inputs do feed into the motion processing system of the neuron, because green-only stimulation clearly led to different activity patterns in the cell compared with the multiple-receptor stimulation provided by the short-wavelength stimulus. For example, spontaneous activity without any specific motion or flash stimuli was always higher with the green-only stimulus (e.g., Fig. 4). The implication here is that the short-wavelength inputs provide a persistent inhibition that prevents the ongoing activity generated by green-only stimulation. When the stimulus moved in the preferred direction, response amplitudes were similar for stimulation with the short-wavelength and green-only stimuli. Had only the green receptors contributed during short-wavelength stimulation, the spectral sensitivity functions would predict that responses would be only 10–20% of the amplitude compared with stimulation with the green-only stimulus. That response amplitudes were equal for the green and short-wavelength stimulus provides strong support for input from short-wavelength receptors.

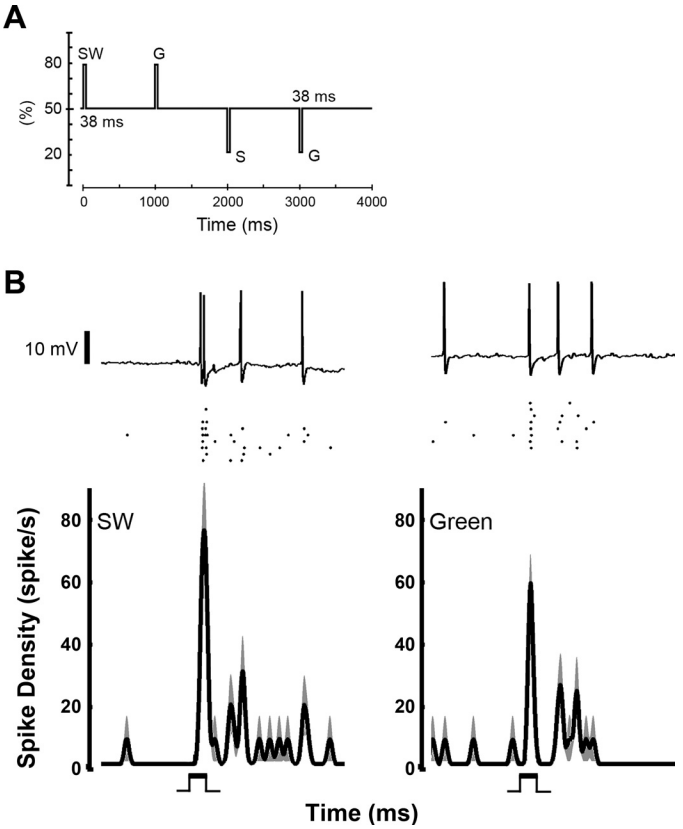

Fig. 7. *A*: the time scale and intensity of flashes with the type II flashed stimulus. The flashed stimulus consisted of increments (80% maximum intensity) or decrements (20% maximum intensity) of either the SW or green (G) LEDs above or below the mean background (50% maximum intensity). The stimulus was 38 ms in duration and 1 s in interval. The sequence of the flashes was SW increment, green increment, SW decrement, and then green decrement. *B* and *C*: $DNII_2$ responses to SW and green brightness increment flashes (*top*, a raw trace; *middle*, raster plot; *bottom*, spike density function). The neuron showed an excitatory response to both SW and green brightness increments.

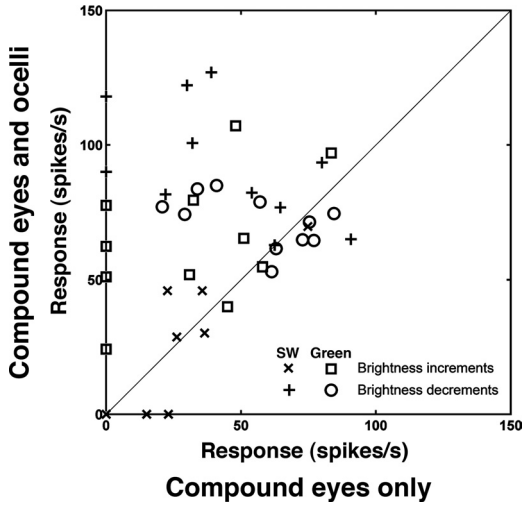

Fig. 8. Plot of response amplitudes with both eye types uncovered as a function of response amplitudes with only the compound eyes uncovered. The responses are to brightness increments with the SW and green stimuli and to brightness decrements for both stimulus types. Across the population, flash responses were larger when both eye types were uncovered.

Although our finding of multiple spectral inputs to a motion-sensitive interneuron contrasts with the dogma that only one type of photoreceptor is involved in motion vision, a very recent study on *Drosophila* motion vision also came to a similar conclusion (Wardill et al. 2012). It was shown that instead of using just one class of photoreceptor (R1–R6, often referred to as the motion channel), the R7 and R8 receptors (often termed the color channel) also contribute to the motion pathway by convergence of all channels at the large monopolar cell level in the optic lobes. This convergence improves motion discrimination. Paulk et al. (2008) showed that in bumblebees, some lobula cells were sensitive to both color and motion, which suggested that although the motion and color information pathways are initially segregated, they converge on the higher order neurons. In honeybees, the convergence of the motion and color information pathways was also proved by behavioral experiments (Stojcev et al. 2011; Zhang et al. 1995).

With different eye regions looking at different portions of a nearly spherical view, the compound eyes of bees are providing a huge amount of visual information at all times. Although the spectral heterogeneity of honeybee ommatida shows that the green photoreceptors distribute equally throughout the compound eye, the UV and the blue channels have different densities in different eye regions (Wakakuwa et al. 2005). In the dorsofrontal region, which we stimulated, the ratio between UV and blue receptors is 3:1. In the midfrontal and lateral regions, the ratio is 2:1. Several behavioral studies have shown that honeybees use different eye regions to detect different colors, forms, and movements (Giger and Srinivasan 1997; Lehrer 1998). In some insects it has been found that the different eye regions are equally involved in optomotor responses (flies: Götz 1964; crickets: Kien 1974). However, the optomotor response of honeybees to horizontal movements was found to exhibit regional specialization across the compound eyes (Moore et al. 1981; Moore and Rankin 1982). The studies showed that honeybees use the ventrolateral regions of the compound eyes for horizontal optomotor responses, whereas the dorsal half of the eye and medial region appeared irrelevant to this behavioral reflex (Moore et al. 1981). With the wide-field LED display used in the present study, the stimuli were restricted to frontal and dorsal eye regions, whereas Kaiser's experiments stimulated the ventral eye regions. We conclude that the optomotor system of the bee does receive input from photoreceptors other than those in the green channel but that this may be regionalized within the compound eyes and may be dependent on the direction of motion being calculated.

Ocellar Input to the Descending Neurons

Previously, recordings from interneurons that receive input from the ocellar retina (ocellar L-neurons) showed that direct stimulation of the ocelli generated robust responses to both short-wavelength and green light (Milde 1984). The ocellar L-neurons have their arborizations in the posterior protocerebrum, where there are dendrites of many descending neurons (Milde and Homberg 1984; Pan and Goodman 1977). Through electrophysiological recordings, it was also shown that at least one type of descending neuron receives inputs from the ocellar L-neurons (Guy et al. 1979). In locusts, the L-neurons were shown through both anatomic and electrophysiological investigations to be connected to descending neurons (Simmons 2002). In the fly, it was also shown that direct synapses between L-neurons and descending neurons exist (Strausfeld and Bassemir 1985). Recent electrophysiological evidence from flies also demonstrates that fusion of compound eye and ocellar sensory information occurs in a pathway that includes the optic lobes (Parsons et al. 2006, 2010).

It is generally believed that the ocellar L-neurons have an important role in modulating descending cell activity and providing an additional, short-latency visual input (Goodman 1981; Guy et al. 1979). In the present study we have established that a prominent descending neuron, which does not itself have dendrites directly in the ocellar retinas, nonetheless receives input from the ocelli. We found that for $DNII_2$ the ocellar input provides a short-latency directional response that adds to a highly direction-selective response generated through inputs from the compound eyes. The directional ocellar input increases the response amplitudes to moving stimuli. The short-latency response suggests a direct input to $DNII_2$ from the ocellar neurons, but a route via the optic lobes is also possible.

Two spectral classes of photoreceptors have been identified in the ocellar retina of the bee, a blue-green-wavelength channel and a UV channel. The peak sensitivities of these channels are around 340 and 500 nm, respectively (Goldsmith and Ruck 1958; Milde 1984). Our short-wavelength stimulus had a peak output at 380 nm, whereas the green LED had a peak at 530 nm. The output of the green LED did not overlap with the spectral sensitivity of the UV receptor, but the short-wavelength stimulus provided approximately equal stimulation to both the UV and blue-green channels. It is interesting that for green brightness increments, responses were often completely absent when the ocelli were covered. This implies that the ocelli may provide a particularly strong drive to the cells during green stimulation.

Recently, it was shown that neurons receiving input from the ocelli of dragonflies are direction selective when stimulated by moving bars of short-wavelength light (peak: 380 nm; van

Kleef et al. 2008). Given that this occurs in another insect species, it is plausible that in the honeybee, the short-wavelength responses of the descending neuron, $DNII_2$, may also receive a directional signal from the ocelli. We have shown that the response amplitudes of $DNII_2$ are only slightly increased when both the compound eyes and ocelli are stimulated simultaneously, compared with only compound eye stimulation. The main impact of the ocellar input is an initial short-latency transient response. The fact that the shorter latency components of the responses are direction selective implies that the ocelli might provide a directional signal. Moreover, a directional component can be observed in the after-responses of $DNII_2$. There are two routes by which a directional signal could arise from the ocelli. The first is that a directional signal is computed in the ocellar retina, as appears to be the case in dragonflies (van Kleef et al. 2008). The second is that input from the median and lateral ocelli may interact to generate a motion signal. In support of the latter notion, it has been shown that signals from the lateral ocelli combine to provide a directional input to a roll-sensitive neuron in the lobula of the fly (Parsons et al. 2006).

ACKNOWLEDGMENTS

We thank Wen-Yen Wu and Pei-Ju Chen for their help with the calculation of the theoretical quantum catch.

DISCLOSURES

No conflicts of interest, financial or otherwise, are declared by the authors.

AUTHOR CONTRIBUTIONS

Y.-S.H., J.P.v.K., G.S., and M.R.I. conception and design of research; Y.-S.H. and M.R.I. performed experiments; Y.-S.H., J.P.v.K., and M.R.I. analyzed data; Y.-S.H. and M.R.I. interpreted results of experiments; Y.-S.H. and M.R.I. prepared figures; Y.-S.H., J.P.v.K., and M.R.I. drafted manuscript; Y.-S.H., J.P.v.K., G.S., and M.R.I. edited and revised manuscript; M.R.I. approved final version of manuscript.

REFERENCES

Autrum HV, von Zwehl VZ. Spektrale Empfindichkeit einzelner Sehzellen des Bienenauges. *Z Vgl Physiol* 48: 357–384, 1964.

Berry RP, Ibbotson MR. A three-dimensional atlas of the honeybee neck. *PLoS One* 5: 1–14, 2010.

Berry R, Stange G, Olberg R, van Kleef J. The mapping of visual space by identified large second-order neurons in the dragonfly median ocellus. *J Comp Physiol A* 192: 1105–1123, 2006.

Boeddeker N, Dittmar L, Stürzl W, Egelhaaf M. The fine structure of honeybee head and body yaw movements in a homing task. *Proc Biol Sci* 277: 1899–1906, 2010.

Boeddeker N, Hemmi JM. Visual gaze control during peering flight manoeuvres in honeybees. *Proc Biol Sci* 277: 1209–1217, 2010.

Giger AD, Srinivasan MV. Honeybee vision: analysis of orientation and colour in the lateral, dorsal and ventral fields of view. *J Exp Biol* 200: 1271–1280, 1997.

Goldsmith TH, Ruck PR. The spectral sensitivities of the dorsal ocelli of cockroaches and honeybees. *J Gen Physiol* 41: 1171–1185, 1958.

Goodman LJ. Organisation and physiology of the insect dorsal ocellar system. In: *Handbook of Sensory Physiology*, edited by Autrum H. Berlin: Springer, 1981, vol. VII/6C, p 201–286.

Goodman LJ, Fletcher WA, Guy RG, Mobbs PG, Pomfrett CJ. Motion sensitive descending interneurons, ocellar LD neurons and neck motor neurons in the bee: a neural substrate for visual course control in *Apis mellifera*. In: *Neurobiology and Behaviour of Honeybees*, edited by Menzel R and Mercer A. Berlin: Springer, 1987, p. 158–171.

Goodman LJ, Ibbotson MR, Bidwell NJ. Spatial, temporal and directional properties of motion-sensitive visual neurons in the honeybee. In: *The Behaviour and Physiology of Bees*, edited by Goodman L and Fisher RC. Oxon, UK: CAB International, 1991.

Goodman LJ, Ibbotson MR, Pomfrett CJ. Directional tuning of motion-sensitive interneurons in the brain of insect. In: *Higher Order Sensory Processing*, edited by Guthrie DM. Manchester, UK: Manchester Univ. Press, 1990.

Götz KG. Optomotorische Untersuchungen des visuellen Systems einiger Augenmutanten der Fruchtfliege *Drosophila*. *Kybernetik* 2: 77–92, 1964.

Guy RG, Goodman LJ, Mobbs PG. Visual interneurons in the bee brain: synaptic organisation and transmission by graded potentials. *J Comp Physiol A* 134:253–264, 1979.

Hertel H, Maronde U. Processing of visual information in the honeybee brain. In: *Neurobiology and Behavior of Honeybees*, edited by Menzel R and Mercer A. Berlin: Springer, 1987, p. 141–157.

Hung YS, van Kleef J, Ibbotson MR. Visual response properties of neck motor neurons in the honeybee. *J Comp Physiol A* 197: 1173–1187, 2011.

Ibbotson MR. A motion-sensitive visual descending neurons in *Apis mellifera* monitoring translator flow-fields in the horizontal plane. *J Exp Biol* 157: 573–577, 1991a.

Ibbotson MR. Wild-field motion-sensitive neurons tuned to horizontal movement in the honeybee, *Apis mellifera*. *J Comp Physiol A* 168: 91–102, 1991b.

Ibbotson MR, Goodman LJ. Response characteristics of four wide-field motion-sensitive descending interneurons in *Apis mellifera*. *J Exp Biol* 148: 255–279, 1990.

Ibbotson MR, Price NS. Spatiotemporal tuning of directional neurons in mammalian and avian pretectal nuclei: similarities of physiological properties. *J Neurophysiol* 86: 2621–2624, 2001.

Ibbotson MR, Price NS, Crowder NA, Ono S, Mustari MJ. Enhanced motion sensitivity follows saccadic suppression in the superior temporal sulcus of the macaque cortex. *Cereb Cortex* 17: 1129–1138, 2007.

Kaiser W. The relationship between visual movement detection and colour vision in insects. In: *The Compound Eye and Vision of Insects*, edited by Horridge A. Oxford, UK: Clarendon Press, 1975.

Kaiser W, Liske E. Die optomotorische Reaktionen von fixiert fliegenden Bienen bei Reizung mit Spektrallichtern. *J Comp Physiol* 89: 391–408, 1974.

Karmeier K, van Hateren JH, Kern R, Egelhaaf M. Encoding of naturalistic optic flow by a population of blowfly motion-sensitive neurons. *J Neurophysiol* 96: 1602–1614, 2006.

Kien J. Sensory integration in the locust optomotor system. II. Direction selective neurons in the circumoesophageal connective and the optic lobe. *Vision Res* 14: 1255–1268, 1974.

Kelber A. Ovipositing butterflies use a red receptor to see green. *J Exp Biol* 202: 2619–2630, 1999.

Kelber A, Balkenius A, Warrant EJ. Colour vision in diurnal; and nocturnal hawkmoths. *Integr Comp Biol* 43: 571–579, 2003.

Kern R, van Hateren JH, Michaelis C, Lindemann JP, Egelhaaf M. Function of a fly motion-sensitive neuron matches eye movements during free flight. *PLoS Biol* 3: 1130–1138, 2005.

Krapp HG, Hengstenberg R. Estimation of self-motion by optic flow processing in single visual interneurons. *Nature* 384: 463–466, 1996.

Künze P. Untersuchung des Bewegungssehens fixiert fliegender Bienen. *Z Vgl Physiol* 44: 656–684, 1961.

Lehrer M. Looking all around: honeybee use different cues in different eye regions. *J Exp Biol* 201: 3275–3292, 1998.

Lindemann JP, Weiss H, Moeller R, Egelhaaf M. Saccadic flight strategy facilitates collision avoidance: closed-loop performance of a cyberfly. *Biol Cybern* 98: 213–227, 2008.

McCann GD, Arnett DW. Spectral and polarization sensitivity of the dipteran visual system. *J Gen Physiol* 59: 534–558, 1972.

Menzel R, Blakers M. Colour receptors in the bee eye-morphology and spectral sensitivity. *J Comp Physiol A* 108: 11–33, 1976.

Menzel R, Ventura DF, Hertel H, de Souza JM, Greggers U. Spectral sensitivity of photoreceptors in insect compound eyes: comparison of species and methods. *J Comp Physiol A* 158: 165–177, 1986.

Milde JJ. Ocellar interneurons in the honeybee. *J Comp Physiol A* 154: 683–693, 1984.

Milde J, Homberg U. Ocellar interneurons in the honeybee: characteristics of spiking L-neurons. *J Comp Physiol A* 155:151–160, 1984.

Moore D, Penikas J, Rankin MA. Regional specialization for an optomotor response in the honeybee compound eye. *Physiol Entomol* 6: 61–69, 1981.

Moore D, Rankin MA. Direction-sensitive partitioning of the honeybee optomotor system. *Physiol Entomol* 7: 25–36, 1982.

Olberg RM. Object and self-movement detectors in the ventral nerve cord of the dragonfly. *J Comp Physiol A* 141: 327–334, 1981a.

Olberg RM. Parallel encoding of direction of wind, head, abdomen and visual pattern movement by single interneurons in the dragonfly. *J Comp Physiol A* 142: 27–41, 1981b.

Olberg RM. Identified target-selective visual interneurons descending from the dragonfly brain. *J Comp Physiol A* 159: 827–840, 1986.

Pan KC, Goodman LJ. Ocellar projections within the central nervous system of the worker honey bee, *Apis mellifera*. *Cell Tissue Res* 176: 505–527, 1977.

Parsons MM, Krapp HG, Laughlin SB. A motion-sensitive neurone responds to signals from the two visual systems of the blowfly, the compound eyes and ocelli. *J Exp Biol* 209: 4464–4474, 2006.

Parsons MM, Krapp HG, Laughlin SB. Sensor fusion in identified visual interneurons. *Curr Biol* 20: 624–628, 2010.

Paulk AC, Phillips-Portillo J, Dacks AM, Fellous JM, Gronenberg W. The processing of color, motion, and stimulus timing are anatomically segregated in the bumblebee brain. *J Neurosci* 28:6319–6332, 2008.

Peitsch D, Fietz A, Hertel H, Desouza J, Ventura DF, Menzel R. The spectral input systems of hymenopteran insects and their receptor-based color vision. *J Comp Physiol A* 170: 23–40, 1992.

Rowell CH, Reichert M. Three descending interneurons reporting deviation from course in the locust. II. Physiology. *J Comp Physiol A* 158: 775–794, 1986.

Schlieper C. Farbensinn der Tiere und optomotorische Reaktion. *Z Vgl Physiol* 6: 453–472, 1927.

Simmons PJ. Signal processing in a simple visual system: the locust ocellar system and its synapses. *Microsc Res Tech* 56: 270–280, 2002.

Singarajah KV. Spectral sensitivity of motion-sensitive units of the butterfly ventral nerve cord. *J Insect Physiol* 119: 1–4, 1988.

Srinivasan MV. Shouldn't directional movement detection necessarily be "colour-blind"? *Vision Res* 25: 997–1000, 1985.

Srinivasan MV, Guy RG. Spectral properties of movement perception in the dronefly *Eristalis*. *J Comp Physiol A* 166: 287–295, 1990.

Stavenga DG, Smits RP, Hoenders BJ. Simple exponential functions describing the absorbance bands of visual pigment spectra. *Vision Res* 33: 1011–1017, 1993.

Stojcev M, Radtke N, D'Amaro D, Dyer AG, Neumeyer C. General principles in motions vision: Color blindness of object motion depends on pattern velocity in honeybee and goldfish. *Vis Neurosci* 28: 361–370, 2011.

Strausfeld NJ, Bassemir UK. Lobula plate and ocellar interneurons converge onto a cluster of descending neurons leading to neck and leg motor neuropil in *Calliphora erythrocephala*. *Cell Tissue Res* 240: 617–640, 1985.

Wakakuwa M, Kurasawa M, Giurfa M, Arikawa K. Spectral heterogeneity of honeybee ommatidia. *Naturwissenschaften* 92: 464–467, 2005.

Wardill TJ, List O, Li X, Dongre S, McCulloch M, Ting CY, O'Kane CJ, Tang S, Lee CH, Hardie RC, Juusola M. Multiple spectral inputs improve motion discrimination in the *Drosophila* visual system. *Science* 336: 925–931, 2012.

Wertz A, Borst A, Haag J. Nonlinear integration of binocular optic flow by DNOVS2, a descending of the fly. *J Neurosci* 28: 3131–3140, 2008.

van Hateren JH, Schilstra C. Blowfly flight and optic flow. II. Head movements during flight. *J Exp Biol* 202: 1491–1500, 1999.

van Kleef J, Berry R, Stange G. Directional selectivity in the simple eye of an insect. *J Neurosci* 28: 1847–2855, 2008.

Yamaguchi S, Wolf R, Desplan C, Heisenberg M. Motion vision is independent of color in Drosophila. *Proc Natl Acad Sci USA* 105: 4910–4915, 2008.

Yamawaki Y, Toh Y. A descending contralateral directionally selective movement detector in the praying mantis *Tenodera aridifolia*. *J Comp Physiol A* 195: 1131–1139, 2009.

Zhang SW, Srinivasan MV. Behavioural evidence for parallel information processing in the visual system of insects. *Jpn J Physiol* 43: S247–S258, 1993.

Zhang SW, Srinivasan MV, Collett T. Convergent processing in honeybee vision: multiple channels for the recognition of shape. *Proc Natl Acad Sci USA* 92: 3029–3031, 1995.